v. 4, n. 12, 2024

Journal of Engineering Research

A STOCHASTIC NUMERICAL APPROACH TO STUDY STAGNATION POINT CARREAU NANOFLUID FLOW IMPACTED BY THERMAL RADIATION AND ACTIVATION ENERGY

Eman Fayz A. Alshehery
Department of Mathematics, Faculty of Science, King Abdulaziz University, Jeddah, Saudi Arabia

Eman Salem Alaidarous
Department of Mathematics, Faculty of Science, King Abdulaziz University, Jeddah, Saudi Arabia

Rania. A. Alharbey
Department of Mathematics, Faculty of Science, King Abdulaziz University, Jeddah, Saudi Arabia

Muhammad Asif Zahoor Raja
Future Technology Research Center, National Yunlin University of Science and Technology, Douliou, Yunlin, Taiwan

Abstract: The motivation behind this research is the great interest that nanofluids have received from scientists and researchers due to their exceptional thermal performance in heat transfer processes. Moreover, employing artificial intelligence and its various technologies to solve real-life problems. This research studies the two-dimensional stagnation point Carreau nanofluid flux (2D-SPCNFF) across a stretching sheet that is impacted by thermal radiation and Arrhenius activation energy. The mathematical formulation of the problem is signified through a nonlinear partial differential equations (PDEs) system that was diminished to a nonlinear ordinary differential equations (ODEs) system by applying the correspondence transformations. The ordinary differential equations ODEs are solved by employing the Lobatto IIIA method using the bvp4c package in MATLAB regarding different values of physical parameters. The solution of ODEs is used as a dataset with nftool technique in MATLAB to design a stochastic numerical approach by the Levenberg Marquardt backpropagation neural networks approach (LMB-NNA). The efficiency, consistency, and convergence of the proposed approach are illustrated by both graphical and numerical consequences using the mean squared error, histograms for error, and linear regression. The performance of the flux velocity, fluid temperature distribution, and fluid concentration of the flow under the effect of the mixed convection parameter, Hartmann number, Ecker number, activation energy parameter, radiation parameter, heat generating parameter, and reaction rate, is shown as a numerical solutions by LMB-NNA for 2D-SPCNFF problem. With rising heat generation parameter, radiation parameter, and Ecker number values, the temperature distribution grows. For the large rate of an activation energy parameter, the concentration increases.

Keywords: Nanofluid; Lobatto IIIA; Levenberg Marquardt; Activation Energy; Thermal Radiation.

INTRODUCTION

Depending on many variables, the velocity of chemical reactions may vary and can be used to interpret the reaction mechanism and the whole process, such as activation energy. Arrhenius popularized the phrase "activation energy" in 1889. The least energy necessary for a chemical reaction to start is called activation energy. Chemical procedures, oil reserves, solar thermal systems, and water emulsification are the industries and fields that utilize activation energy. The chemical processes and activation energy characteristics of the magneto nanofluid were surveyed by (Mustafa et al. (2017)). A stretched surface was utilized by (Hayat et al. (2020)) to analysis the influence of an Arrhenius activation energy upon the flow of a 3D MHD nanofluid. Using thermal radiation, (Sajid et al. (2018)) examined the Maxwell Darcy-Forchheimer nanofluid flow impacted by the activation energy. (Kahn et al. (2020)) considered the effect of the Arrhenius activation energy upon the Casson nanofluid flux. (Alsaadi et al. (2020)) analyzed Williamson nanofluid flux with the impact of activation energy. (Bhatti et al. (2020)) conducted a study to examine the motion of gyrotactic microorganisms in a magnetized nanofluid through a porous plate that is impacted by activation energy on. The consequences of activation energy on 2D nanofluid flux with heat and mass transfer were observed by (Kalaivanan et al. (2020)).

Thermal radiation is a form of electromagnetic radiation produced when particles in matter move due to their temperature. Thermal radiation is formed if thermal energy from the motion of charges in the material (protons and electrons) is

NOMENCLATURE

PDEs	Partial differential equations	*SPCNFF*	stagnation point Carreau nanofluid flow
2D	Tow-dimensional	*MSE*	Mean Squared Error
LMBNNA	Levenberg Marquardt backpropagation neural network approach	*ODEs*	Ordinary differential equations
M	Hartmann number	(u,v)	Velocity components
$\in$	Reaction rate	B_0	Magnetic parameter
E	Activation energy parameter	δ	Heat generating parameter
λ	Mixed convection parameter	Ec	Ecker number
A	Speed ratio	ν_f	Kinematic viscosity
(x,y)	Cartesian coordinates	T_w	Surface temperature
Bi	Biot number	σ	Electric conductivity
T	Fluid temperature	U_w	Stretching velocity
Nt	Thermophoresis	R	Radiation parameter
θ_w	Temperature ratio parameter	Nu	Local Nusselt number
E_a	Activation energy	k	Thermal conductivity
γ	Chemical reaction constant	ψ	Stream function
N	buoyancy ratio parameter	λ_1	Weissenberg number
f	Dimensionless stream function	α_m	Thermal diffusivity
C_w	Surface volume fraction	T_∞	Ambient temperature
S	Suction parameter	U_∞	Free stream velocity
C_f	Skin friction coefficient	φ	Dimensionless concentration
Pr	Prandtl number	Nb	Brownian motion
Re	Local Reynolds number	ρ	Fluid density
C	Fluid concentration	C_∞	Ambient concentration
K_1	Free stream velocity	μ	Dynamic viscosity
U_0	reference velocity	θ	Dimensionless temperature
n	Power law index	τ_w	Surface shear stress
C_p	specific heat	η	Dimensionless similarity variable
D_B	Brownian diffusion variable	β_t	Thermal expansion coefficient
D_T	Thermophoretic diffusion factor	β_c	Concentration expansion coefficient
q_r	Radiation heat flux	Q_0	heat generation co-efficient
m	Dimensionless rate constant	Sc	Schmidt number
g	Gravity	λ^*	Time constant
u_e	constant reaction rate	c	Free streaming rapidity

transformed into electromagnetic radiation. (Howell et al. (2020)) presented the main physics concepts underlying the phenomenon of thermal radiation. In a vertical wavy porous cavity, the impact regarding thermal radiation upon the bioconvection flux of nanofluid and oxytactic microorganisms was analyzed by (Hussain et al. (2022)). Nanofluid is simulated parametrically subject to thermal radiation through a porous shrinking/stretching sheet by (Bilal et al. (2022)). Entropy production in a nanofluid affected by thermal radiation and the Cattaneo-Christov model was studied numerically by (Waqas et al. (2022)). (Shaw et al. (2022)) studied the hydromagnetic flux of a Cross hybrid nanofluid that is influenced by linear, nonlinear, and quadratic thermal radiations.

In a fluid stream, a stagnation point is a place where the flux velocity is zero on the top of a submerged surface. (Ramzan et al. (2022)) exhibited the thermodynamics of the stagnation point flux regarding nanofluid. (Haq et al. (2022)) directed the examination of the stagnation point flux for the hydromagnetic nanofluid along a vertical sheet using a modified Chebyshev collocation approach. The heat flux of 2D fluid flow involving stagnation point stream was demonstrated by (Awan et al. (2022)). The heat transmission of electromagnetic fluid flow at the stagnation point was examined by (Bai et al. (2022)).

A generalized Newtonian fluid whose viscosity depends on the shear rate known as Carreau fluid. Carreau first derived from molecular network theories to report rheological equations. The Carreau viscosity model helps characterize the flux performance of fluids in the extreme shear rate zone. The efficiency of nonhomogeneous heat production and the thermodynamics of a Carreau fluid flow along a nonlinear extending cylinder is analyzed by (Hussain et al. (2022)). (Rehman et al. (2022)) presented a theoretical analysis of heat transport in Magnetohydrodynamic thermally slip Carreau fluid. (Reedy et al. (2022)) performed a numerical investigation regarding Carreau fluid flux along a vertical microchannel porous through entropy production. (Qayyum et al. (2022)) investigated the analysis of a magnetohydrodynamic Carreau fluid flow influenced by the heat transfer across a stretched surface. (Shoaib et al. (2022)) studied the flow characteristics of the magnetohydrodynamic Carreau nanofluid model through a numerical intelligent computing algorithm. (Uddin et al. (2022)) inspected the thin film flux of Carreau nanofluid across an extended sheet by using the supervised neural network method.

The first research using the word "nanofluid" was published in 1995 via (Choi & Eastman (1995)). A nanofluid is a combination of ethylene glycol, water, and other base fluids suspended with nanoscale particles. Due to their potential use in several industries, such as computer engineering, thermodynamic systems, solar energy, cooling procedures, heating methods, and thermoelectric devices, nanoparticles have attracted much interest. In a w-form tube under the influence of curvature, (Zaman et al. (2021)) examined blood flow as a non-Newtonian nanofluid. (Uddin et al. (2020)) laid the groundwork for the numerical solutions of magnetic blood nanofluid flow via a cylindrical tube. (Shoaib et al. (2022)) considered the flux properties and heat transmission across a stretched and rotating disk in an unsteady 3D hybrid nanofluid flow. By applying the Buongiorno model, (Hamid et al. (2021)) characterized the Cross-nanofluid flow toward a radially shrinking sheet.

A new stochastic numerical approach for training the ANN is the Levenberg-Marquardt back propagation neural network

approach LMBNNA, which may be used to solve fluid flow problems. To study the magnetohydrodynamic Casson nanofluid with the Darcy-Forchheimer law impacted by mass and heat transmission and the activation energy, (Shoaib et al. (2022)) employed Levenberg Marquardt backpropagation neural network approach. The Levenberg-Marquardt backpropagation neural network approach LMBNNA was used by (Ilyas et al. (2021)) to study the thermodynamic properties of several nanofluidic systems on stretched disks. The flux of the Maxwell nanofluid flow along a stretched and rotating surface under the effect of magnetic and nonlinear thermal radiation was considered by (Uddin et al. (2021)) using Levenberg-Marquardt backpropagated neural network approach.

The two-dimensional stagnation point Carreau nanofluid flux 2D-SPCNFF along a stretching sheet that is affected by thermal radiation and activation energy is numerically examined in this work using a new stochastic numerical approach depending upon Levenberg-Marquardt backpropagation neural networks approach LMBNNA through the MATLAB software by using nftool package.

In section 2, the 2D-SPCNFF problem model is explained. Section 3 details the solution methodology for the innovative approach LMBNNA. The numerical and graphical results of LMBNNA and the impacts of various physical components on the performance of the flux velocity $f'(\eta)$, fluid temperature spreading $\theta(\eta)$, and fluid concentration $\phi(\eta)$ of the flux are discussed in Section 4.

PROBLEM FORMULATION

Consider the thermal radiation and activation energy impacts of an incompressible two-dimensional stagnating point Carreau fluid flux over a stretched surface. To evaluate flow, combined convection is employed. As shown in **Figure 1**, the flow happens in $y > 0$; the surface velocity is $u_w = ax$, $a > 0$, where x-axis is extended regarding the surface.

Assume that surface concentration, surface temperature, ambient concentration, and ambient temperature are C_w, T_w, C_∞ and T_∞, respectively.

For the flow model, the leading partial differential equations PDEs are (Ijaz Khan et al. (2020) & Hayat et al. (2017))

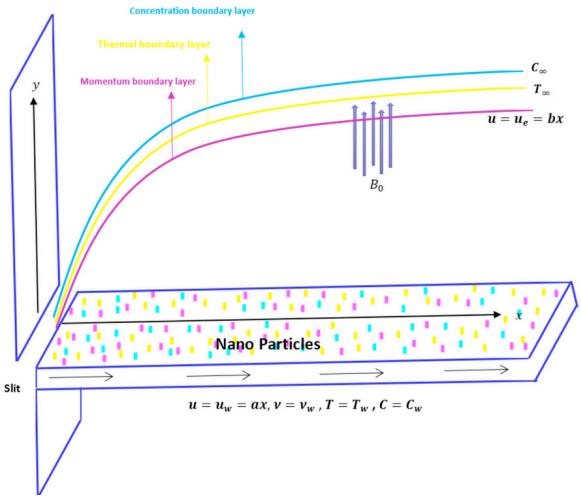

Figure 1. Flow diagram

$$\frac{\partial v}{\partial y}+\frac{\partial u}{\partial x}=0, \tag{1}$$

$$\begin{aligned} v\frac{\partial u}{\partial y}+u\frac{\partial u}{\partial x}=u_e\frac{du_e}{dx}+v_f\frac{\partial^2 u}{\partial y^2}\left[1+\left(\frac{n-1}{2}\right)\lambda^{*^2}\left(\frac{\partial u}{\partial y}\right)^2\right] \\ +(B_c(C-C_\infty)+B_t(T-T_\infty))g \\ +(n-1)v_f\lambda^{*^2}\left[\frac{\partial^2 u}{\partial y^2}\left(\frac{\partial u}{\partial y}\right)^2\right]\left[1+\left(\frac{n-3}{2}\right)\lambda^{*^2}\left(\frac{\partial u}{\partial y}\right)^2\right]+\frac{\sigma {B_0}^2}{\rho}(u_e-u), \end{aligned} \tag{2}$$

$$\begin{aligned} u\frac{\partial T}{\partial x}+v\frac{\partial T}{\partial y}=\alpha_f\frac{\partial^2 T}{\partial y^2}+\tau\left[D_B\frac{\partial C}{\partial y}\frac{\partial T}{\partial y}+\frac{D_T}{T_\infty}\left(\frac{\partial T}{\partial y}\right)\right]-\frac{1}{\rho_f C_p}\frac{\partial q_r}{\partial y} \\ +\frac{\sigma_f {B_0}^2}{\rho_f C_p}(u_e-u)^2+Q_0(T-T_\infty), \end{aligned} \tag{3}$$

$$\begin{aligned} u\frac{\partial C}{\partial x}+v\frac{\partial C}{\partial y}=D_B\frac{\partial^2 C}{\partial y^2}+\frac{D_T}{T_\infty}\frac{\partial^2 T}{\partial y^2}-kr^2 \\ (C-C_\infty)\left(\frac{T}{T_\infty}\right)^m\exp\left[\frac{-E_a}{kT}\right] \end{aligned} \tag{4}$$

The boundary conditions are

$$v = v_w(x), u = u_w(x) = ax, C = C_w, T = T_w, \quad \text{at } y = 0 \tag{5}$$

$$v \to 0, u \to u_e(x) = bx, C \to C_\infty, T \to T_\infty, \quad \text{as } y \to \infty \tag{6}$$

By using the dimensionless variables

$$\eta = y\sqrt{\frac{a}{v}}, \theta(\eta) = \frac{T - T_\infty}{T_w - T_\infty}, \varphi(\eta) = \frac{C - C_\infty}{C_w - C_\infty}, \\ u = axf'(\eta), v = -\sqrt{av}f(\eta) \tag{7}$$

Equations (1)-(4) becomes

$$f'''\left(1+\left(\frac{n-1}{2}\right)\lambda_1(f'')^2\right)+2\left[\left(\frac{n-1}{2}\right)\lambda_1(f'')^2\right]\left[1+\left(\frac{n-3}{2}\right)\lambda_1(f')^2\right] \\ +ff''-(f')^2+\lambda(\theta+N\varphi)+M^2(A-f')+A^2=0, \tag{8}$$

$$\theta''+\Pr f\theta'+\Pr Nb\theta'\varphi'+\Pr Nt\theta'^2+R\left[1+(\theta_w-1)\theta\right]^3\theta''+3R\left[1+(\theta_w-1)\theta\right]^2 \\ (\theta_w-1)\theta'^2+\Pr Ec\left[M^2(A-f')^2+(f'')^2\right]+\Pr\delta\theta=0, \tag{9}$$

$$\varphi''+Scf\varphi'+\frac{Nt}{Nb}\theta''-\varepsilon Sc\varphi\left[1+(\theta_w-1)\theta\right]^m \\ \exp\left[\frac{-E}{1+(\theta_w-1)\theta}\right]=0, \tag{10}$$

With

$$f(0)=S, f'(0)=1, \theta(0)=1, \varphi(0)=1 \\ f'(\infty)=A, \theta(\infty)=0, \varphi(\infty)=0 \tag{11}$$

SOLUTION METHODOLOGY

The following steps describe the solution methodology.

Regarding various values of physical factors, including the mixed convection parameter (λ), Hartmann number (*M*), Ecker number (*Ec*), activation energy parameter (*E*), radiation parameter (*R*), heat generating parameter (*δ*), and reaction rate (∈) as shown in **Table 1**, the approximate solution for the tow-dimensional stagnation point Carreau nanofluid flow 2D-SPCNFF model is calculated by solving ODEs (8-10) with the boundary conditions (11-12).

The suggested Levenberg-Marquardt backpropagation neural networks approach LMBNNA is applied to analyze the numerical solution of the 2D-SPCNFF model using forty neurons, with 80% of the dataset being employed regarding training, 10% regarding validation, and 10% regarding testing in the MATLAB software through nftool package. **Figure 2** displays a 2D-SPCNFF artificial neural network design.

The stability, accuracy, and convergence of the LMBNN approach are shown numerically and graphically in the next section using the mean squared error of performance, histograms for error, gradient value, and linear regression.

Displayed are the effects of various parameters on the performance of the flux velocity $f(\eta)$, fluid temperature spreading $\theta(\eta)$, and fluid concentration $\phi(\eta)$ functions, respectively.

Figure 3 represents all of the previous steps.

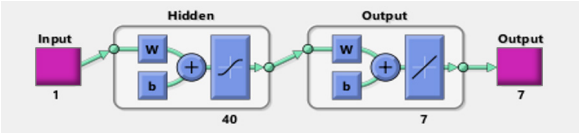

Figure 2. The designed scheme about artificial neural network regarding 2D-SPCNFF

Scenario	Physical parameters	Case 1	Case 2	Case 3	Case 4
1	*M*	1	1.5	2	2.5
2	*λ*	0	0.1	0.2	0.3
3	*Ec*	0	1	2	3
4	*R*	0	0.3	0.6	0.9
5	*δ*	0	0.1	0.2	0.3
6	*E*	3	4	5	6
7	∈	0	0.2	0.4	0.6

Table : Several physical parameters values for 2D-SPCNFF.

OUTCOMES AND DISCUSSION

The review about the numerical and graphical outcomes about the designed Levenberg-Marquardt backpropagation neural network approach LMBNNA regarding the stagnation point two-dimensional Carreau nanofluid flux model is covered in this section.

Figure 4 and **Table 2** provide the graphical and numerical findings of LMBNNA for cases of the Hartmann number M for the velocity f'. For case 3 of scenario 1 the greatest performance has a mean square error value of 10^{-9} at 176 iterations, according to **Figure 4(a)**. The LMBNNA is convergent through the gradient result is and the mu value is 10^{-10} as shown in **Figure 4(b)**. **Figure 4(c)** illustrates the distribution of the error histogram as . The value $R=1$ in the regression analysis plot was displayed in **Figure 4(d)**. The error behavior by function fit plot was presented in **Figure 4(e)**.

The results of the LMBNN approach for the velocity function f' with the case of the mixed convection parameter λ are shown in **Figure 5** and **Table 3**. In case 1 of scenario 2, the mean squared error of the performance was the least, reaching 10^{-8} after 252 iterations, as illustrated in **Figure 5(a)**. The convergence of the LMBNNA using the mu and gradient values that were determined in **Figure 5(b)**. **Figures 5(c,e)** present the error analysis between the output and target of LMBNNA with both the error histogram and function fit plot. The stability of the LMBNNA is discussed in **Figure 5(d)** using the linear regression analysis.

The findings of the LMBNN approach for scenario 3 with case 4 are provided in **Table 4** and **Figure 6**. **Figure 6(a)** shows a plot of the performance with the highest value being 10^{-9} at 57 iterations. **Figure 6(b)** indicates that the mu parameter value is 10^{-10} and the gradient result is . The histogram distribution for error is examined in **Figure 6(c)** with 20 bins. **Figure 6(d)** presents the value $R=1$ for training, testing, validation, and all processes in the linear regression. **Figure 6(e)** displays the function fit plot of LMBNNA.

For case 1 of scenario 4, **Table 5** depicts the mean squared error about testing, training, and validation, gradient value, performance, number of epochs, mu parameter, and processing time.

Figure 7(a-e) shows the accuracy, convergence, and stability of the LMBNN approach for case 1 of scenario 4. The error between the target and output is in the error histogram plot, 10^{-4} in the function fit plot, and the value $R=1$ in the linear regression plot. The mean squared error of performance is 10^{-9} after 144 iterations, the gradient is, and the mu parameter is 10^{-11}.

The numerical findings are provided in **Table 6** for solving situations of the heat generating parameter δ for the temperature \theta, while the graphical outcomes are displayed in Figure 8. (a-e). The best performance is 10^{-8} at 75 epochs. According to the training state plot, the gradient value is and the mu value is 10^{-11}. The error between the output and target is introduced by the error histogram plot is . The regression scheme represents the linear connection between the target data and output. In the function fit plot, the error is 10^{-4}.

The analytical and graphical results about LMBNNA for solving the concentration function ϕ at the cases of the activation energy parameter E are given in **Table 7** and **Figure 9**. For case 4 of scenario 6, **Figure 9(a)** shows the maximum MSE performance is 10^{-11} at 124 iterations. **Figure 9(b)** demonstrates that the gradient result is and the mu value is 10^{-12}. The range of the error histogram is as shown in **Figure 4(c)**. The linear regression plot of the LMBNNA being stable, as illustrated in **Figure 9(d)**, has a value of $R=1$. **Figure 9(e)** displays the error through the function fit plot.

For the reaction rate with the concentration ϕ, the results of the LMBNN approach are displayed in **Figure 10** and **Table 8**, respectively. For case 2 of scenario 7, the lowest mean square error reached 10^{-11} after 159 iterations, as presented in Figure **10(a)**. Using the given mu and gradient values, Figure **10(b)** illustrates the convergence of

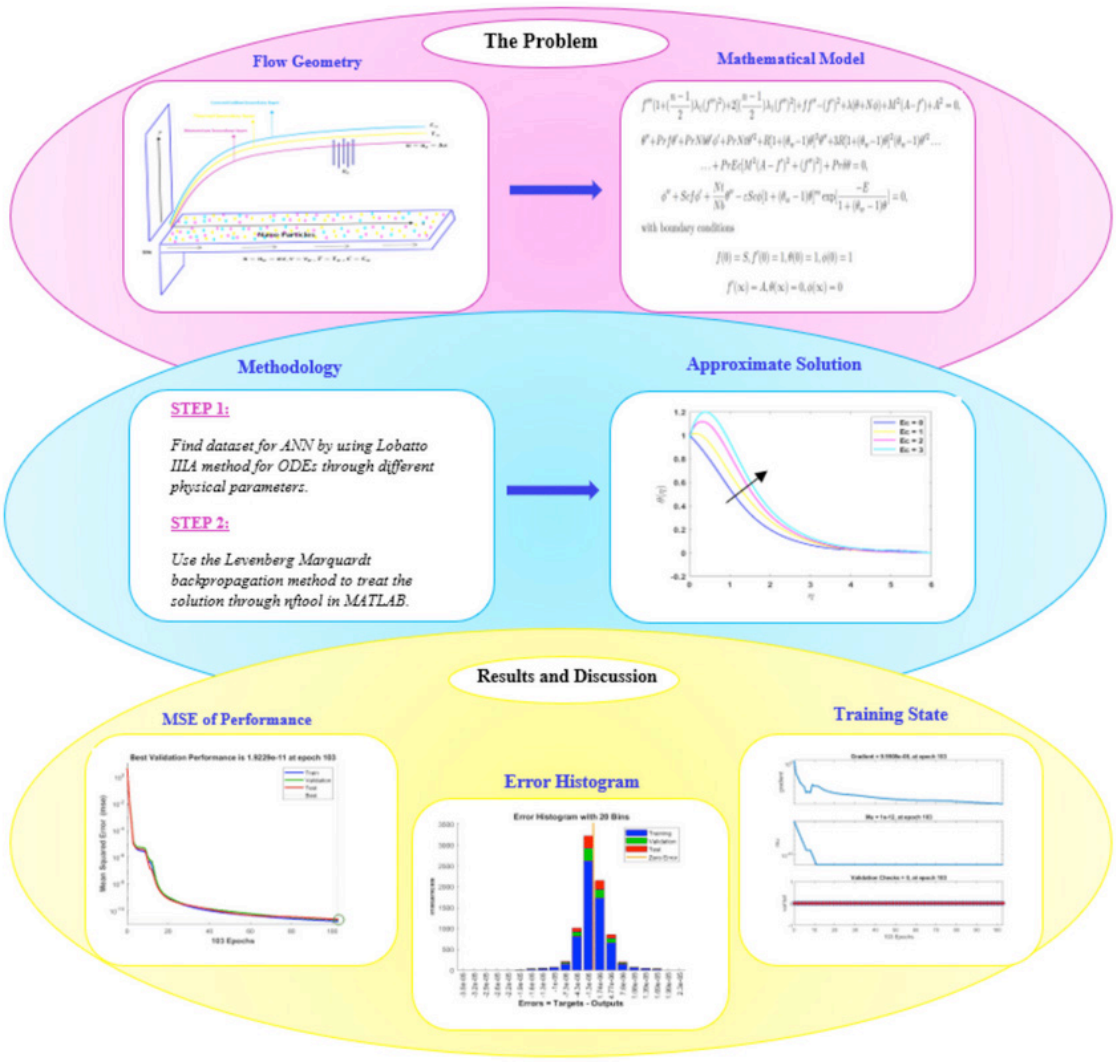

Figure 3. Scheme of solution methodology for 2D-SPCNFF

Scenario	Cases	Mean Squared Error			Performance	Mu Parameter	Gradient	Epochs	Time
		Training	Validation	Testing					
S1	C1	8.32E-08	5.42E-08	9.75E-08	8.30E-08	1.00E-09	6.87E-05	447	7s
	C2	4.14E-08	5.30E-08	5.14E-08	4.14E-08	1.00E-07	1.30E-04	389	6s
	C3	3.91E-09	4.17E-09	8.58E-09	3.39E-09	1.00E-10	3.83E-07	182	3s
	C4	5.84E-09	3.62E-09	8.22E-09	5.84E-09	1.00E-10	6.49E-06	344	5s

Table 2: Numerical findings of LMBNNA regarding scenario 1 about 2D-SPCNFF.

Scenario	Cases	Mean Square Error			Performance	Mu Parameter	Gradient	Epochs	Time
		Training	Validation	Testing					
S2	C1	9.66E-09	1.83E-08	1.72E-08	9.66E-09	1.00E-11	3.24E-06	258	4s
	C2	1.05E-07	4.96E-08	6.98E-08	1.03E-07	1.00E-10	9.71E-05	235	4s
	C3	3.83E-08	4.54E-08	7.28E-08	3.83E-08	1.00E-08	1.31E-06	565	11s
	C4	4.81E-09	5.72E-09	8.02E-09	4.81E-09	1.00E-09	1.39E-06	241	4s

Table 3: Numerical findings of LMBNNA regarding scenario 2 about 2D-SPCNFF.

Scenario	Cases	Mean Square Error			Performance	Mu Parameter	Gradient	Epochs	Time
		Training	Validation	Testing					
S3	C1	1.35E-09	2.45E-09	1.33E-09	1.35E-09	1.00E-09	1.59E-07	643	10s
	C2	7.99E-08	8.38E-08	1.47E-07	7.89E-08	1.00E-10	3.85E-05	318	5s
	C3	7.79E-08	5.45E-08	5,86E-08	7.79E-08	1.00E-10	1.28E-06	174	2s
	C4	4.46E-09	5.66E-09	4.92E-09	3.50E-09	1.00E-10	1.29E-06	63	1s

Table 4: Numerical findings of LMBNNA regarding scenario 3 about 2D-SPCNFF.

Scenario	Cases	Mean Square Error			Performance	Mu Parameter	Gradient	Epochs	Time
		Training	Validation	Testing					
S4	C1	1.47E-10	1.78E-10	2.12E-10	1.47E-10	1.00E-12	9.96E-08	144	2s
	C2	8.98E-08	6.59E-08	1,03E-07	8.92E-08	1.00E-09	3.07E-06	315	6s
	C3	1.60E-08	2.11E-08	3.36E-08	1.60E-08	1.00E-09	3.10E-05	175	3s
	C4	2.17E-07	4.19E-07	1.88E-07	2.15E-07	1.00E-09	1.55E-06	128	2s

Table 5: Numerical findings of LMBNNA regarding scenario 4 about 2D-SPCNFF.

Scenario	Case	Mean Square Error			Performance	Mu Parameter	Gradient	Epochs	Time
		Training	Validation	Testing					
S5	C1	3.27E-08	5.38E-08	4.18E-08	3.27E-08	1.00E-09	9.95E-09	101	1s
	C2	4.42E-09	3.50E-09	5.91E-09	4.42E-09	1.00E-11	1.28E-05	81	1s
	C3	2.01E-07	3.07E-07	2.37E-07	2.01E-07	1.00E-09	5.12E-05	325	5s
	C4	9.83E-09	7.62E-09	7.84E-09	9.82E-09	1.00E-09	2.96E-05	242	4s

Table 6: Numerical findings of LMBNNA regarding scenario 5 about 2D-SPCNFF.

Scenario	Case	Mean Square Error			Performance	Mu Parameter	Gradient	Epochs	Time
		Training	Validation	Testing					
S6	C1	4.16E-12	3.92E-12	4.08E-12	4.16E-12	1.00E-12	8.89E-08	218	4s
	C2	1.52E-12	1.92E-11	2.08E-12	1.51E-12	1.00E-12	9.95E-08	103	3s
	C3	1.05E-12	1.46E-12	1.57E-12	1.05E-12	1.00E-12	9.61E-08	135	3s
	C4	1.33E-12	1.36E-12	1.60E-12	1.33E-12	1.00E-13	9.82E-08	124	4s

Table 7: Numerical findings of LMBNNA regarding scenario 6 about 2D-SPCNFF.

Scenario	Case	Mean Square Error			Performance	Mu Parameter	Gradient	Epochs	Time
		Training	Validation	Testing					
S7	C1	2.38E-12	4.19E-12	6.34E-12	2.38E-12	1.00E-12	9.76E-08	86	1s
	C2	9.63E-12	1.41E-11	1.45E-11	9.63E-12	1.00E-12	9.74E-08	159	2s
	C3	1.23E-12	2.31E-12	1.88E-12	1.23E-12	1.00E-13	9.89E-08	129	2s
	C4	9.35E-10	8.34E-10	9.59E-11	9.33E-11	1.00E-10	1.71E-08	135	2s

Table 8: Numerical findings of LMBNNA regarding scenario 7 about 2D-SPCNFF.

the LMBNNA. The function fit plot and error histogram for the LMBNNA error analysis are shown in **Figures 5(c,e)**. **Figure 5(d)** uses the output and target relationship formed by linear regression analysis to illustrate the accuracy of LMBNNA.

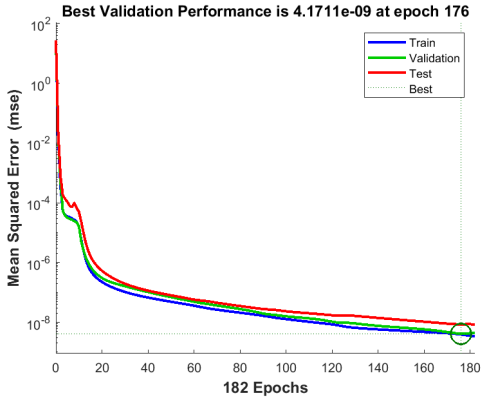

a) MSE of performance about case 3

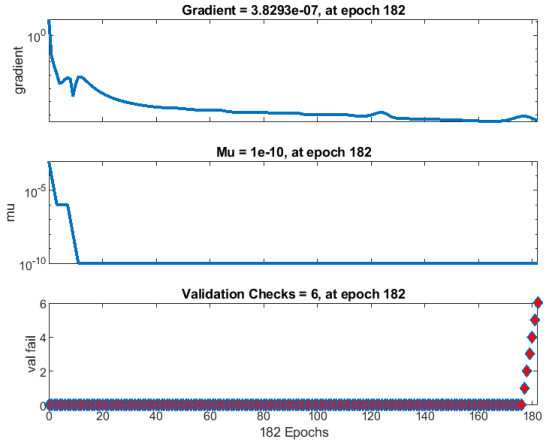

b) Gradient plot about case 3

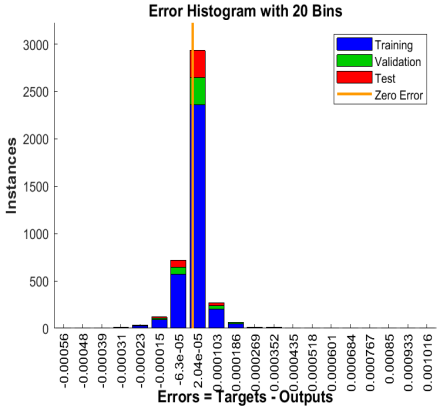

c) Error histogram plot about case 3

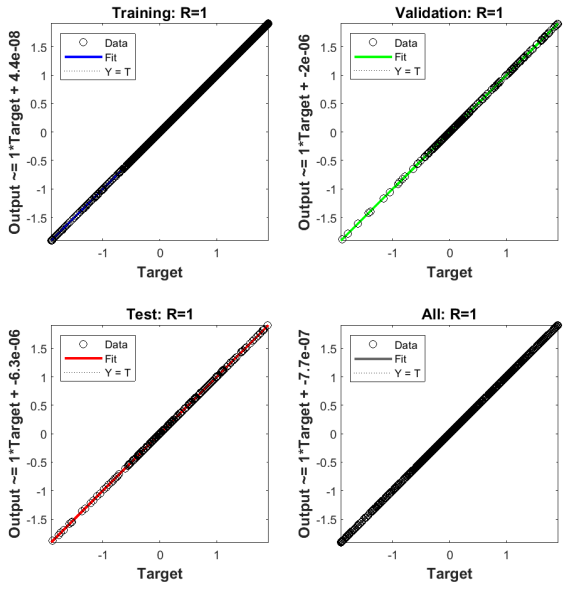

d) Regression plot about case 3

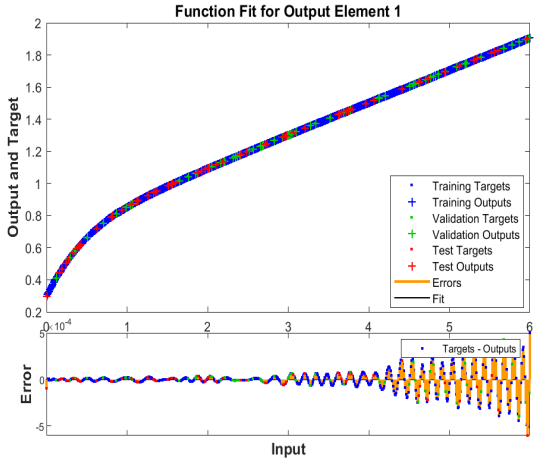

e) Function fit plot about case 3

Figure 4. Graphical outcomes of LMSNN for case 3 of scenario 1 for 2D-RCNFF.

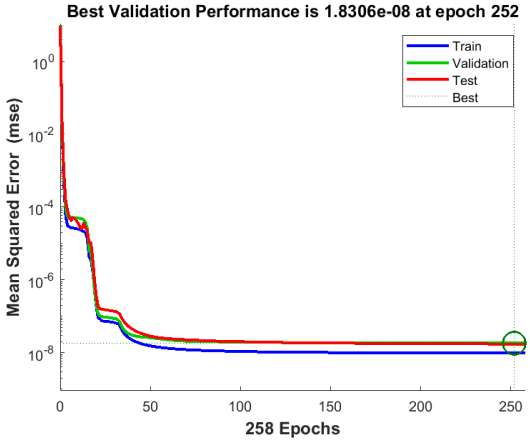

a) MSE of performance about case 1

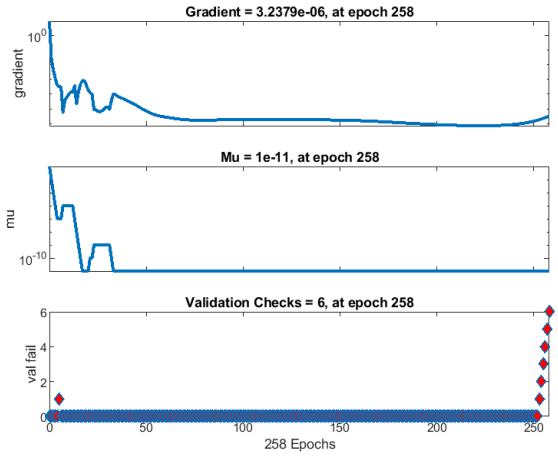

b) Gradient plot about case 1

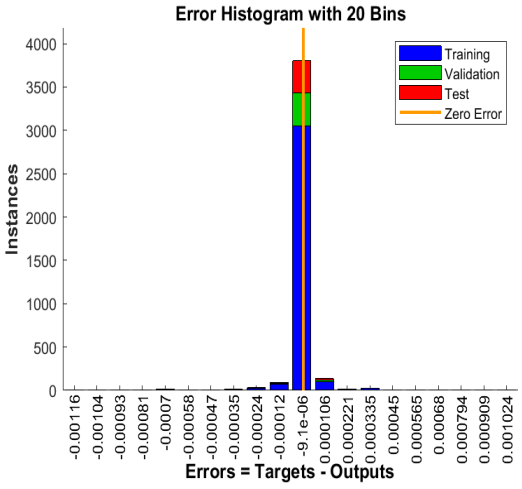

c) Error histogram plot about case 1

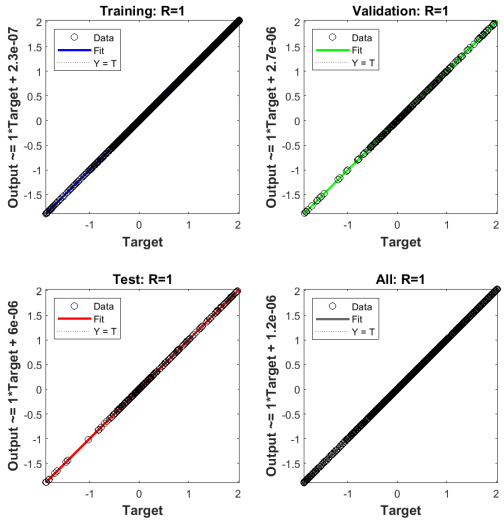

d) Regression plot about case 1

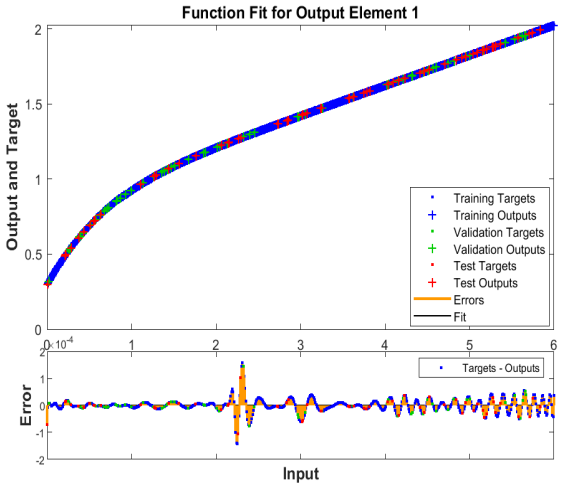

e) Function fit plot about case 1

Figure 5. Graphical outcomes of LMBNNA for case 1 of scenario 2 for 2D-SPCNFF.

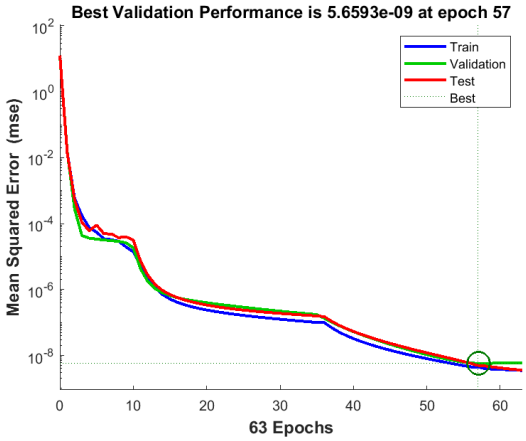

a) MSE of performance about case 4

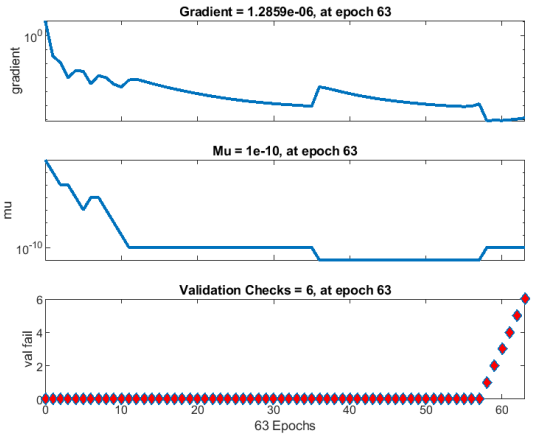

b) Gradient plot about case 4

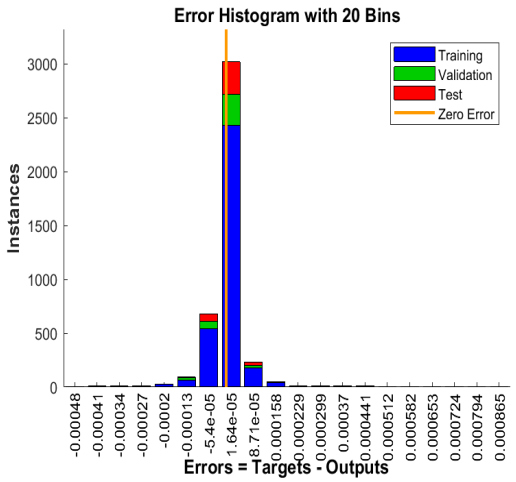

c) Error histogram plot about case 4

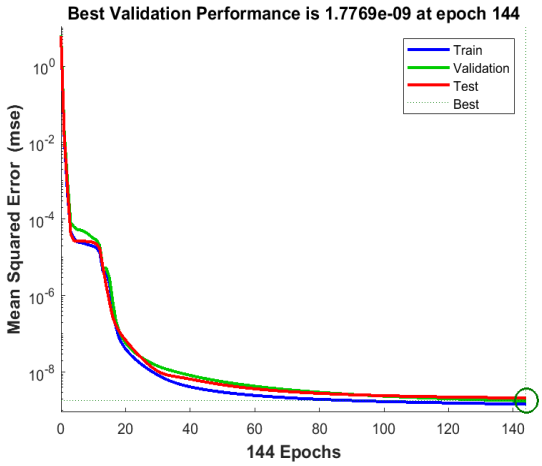

a) MSE of performance about case 1

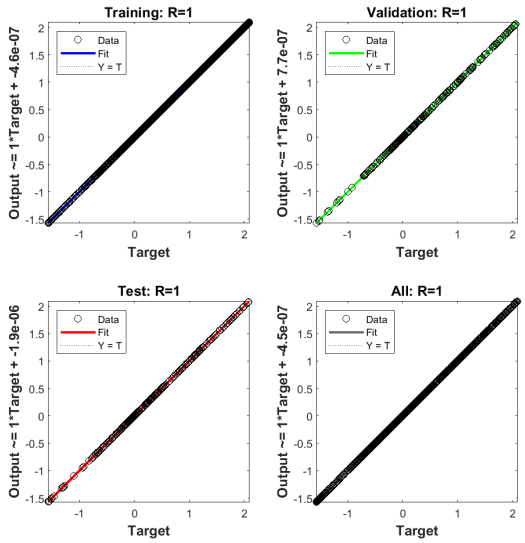

d) Regression plot about case 4

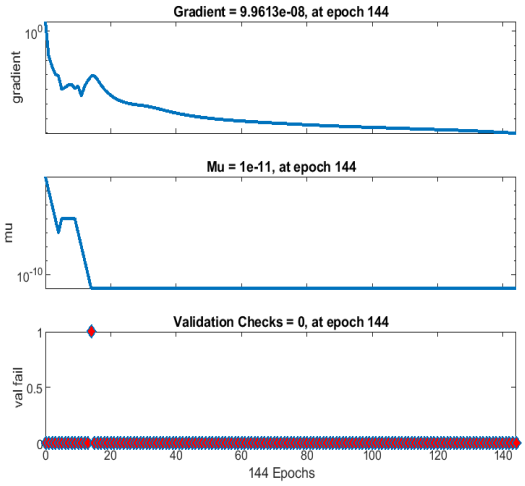

b) Gradient plot about case 1

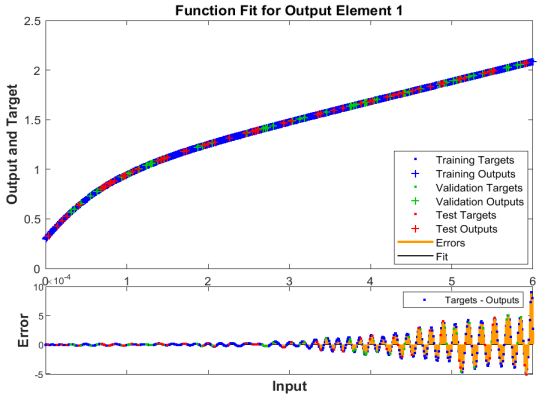

e) Function fit plot about case 4

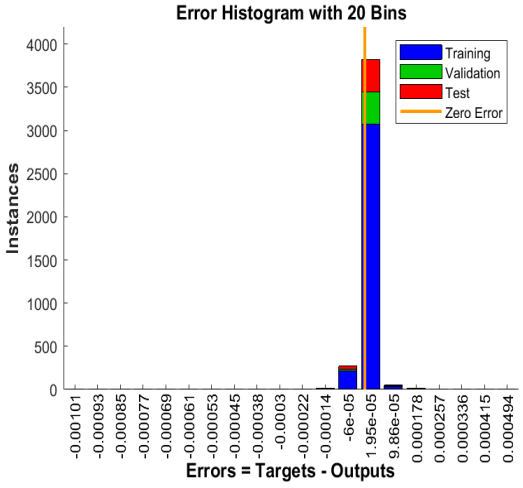

c) Error histogram plot about case 1

Figure 6. Graphical outcomes of LMBNNA for case 4 of scenario 3 for 2D-SPCNFF.

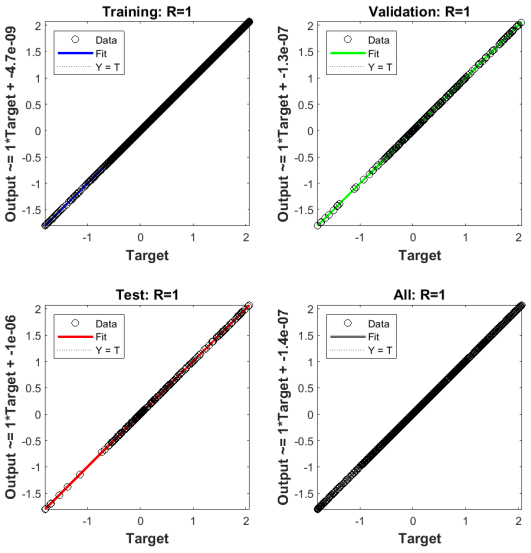

d) Regression plot about case 1

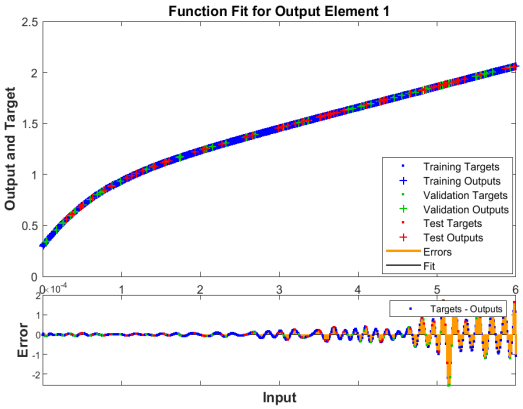

e) Function fit plot about case 1

Figure 7. Graphical outcomes of LMBNNA for case 1 for scenario 4 for 2D-SPCNFF.

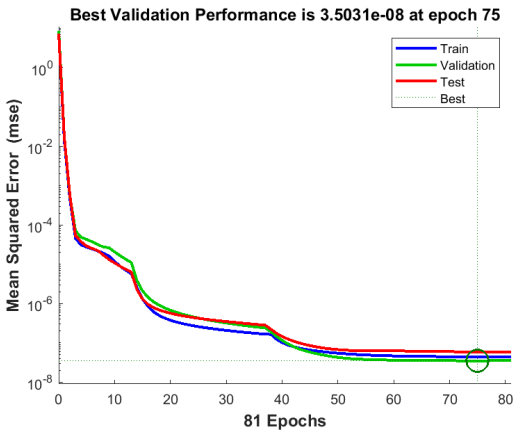

a) MSE of performance about case 2

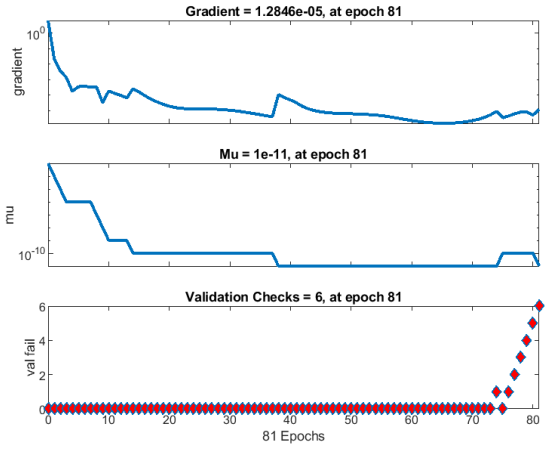

b) Gradient plot about case 2

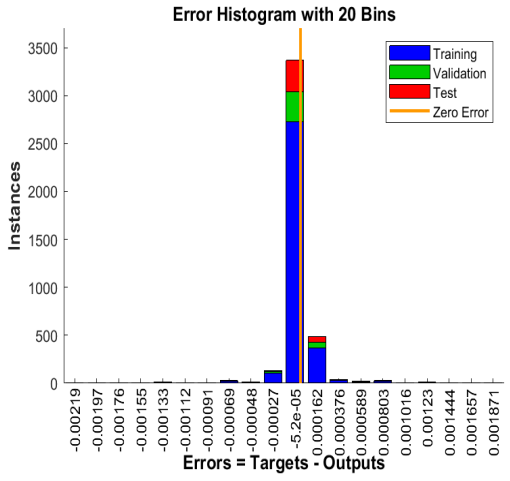

c) Error histogram plot about case 2

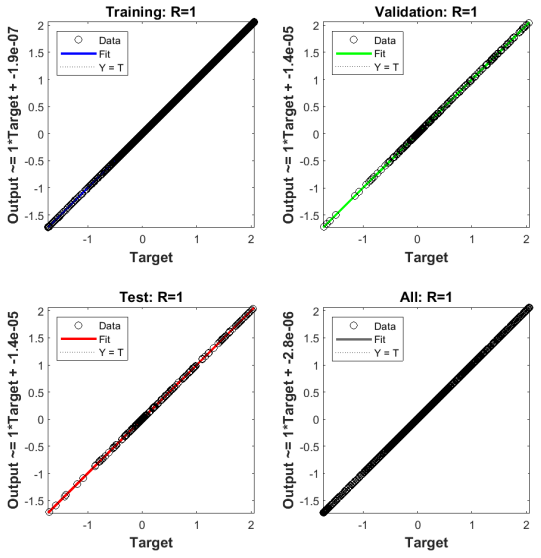

d) Regression plot about case 2

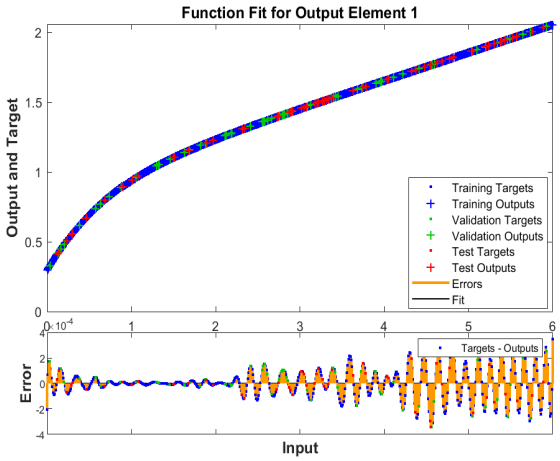

e) Function fit plot about case 2

Figure 8. Graphical outcomes of LMBNNA for case 2 of scenario 5 for 2D-SPCNFF.

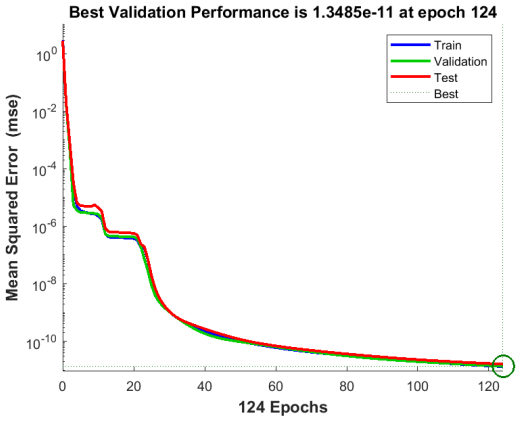

a) MSE of performance about case 4

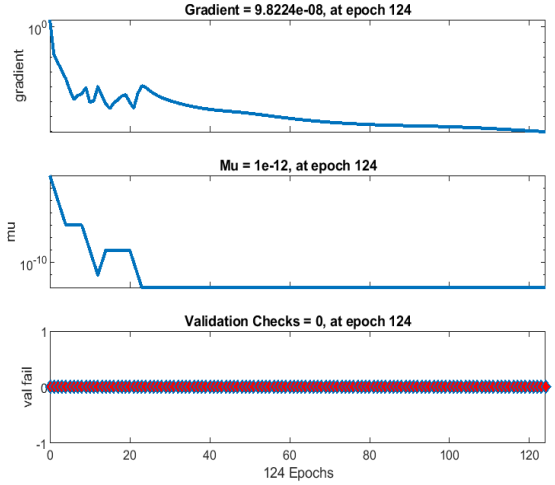

b) Gradient plot about case 4

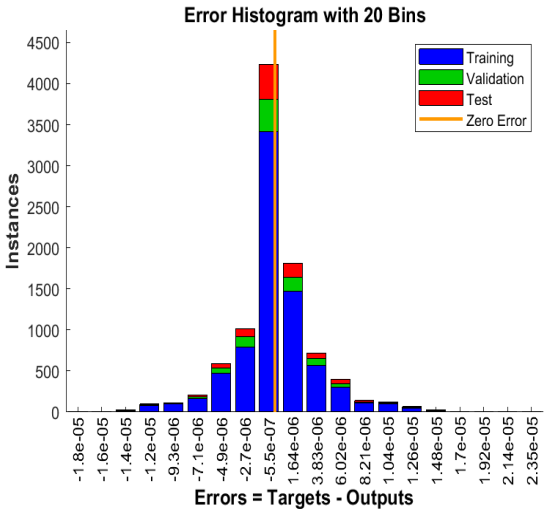

c) Error histogram plot about case 4

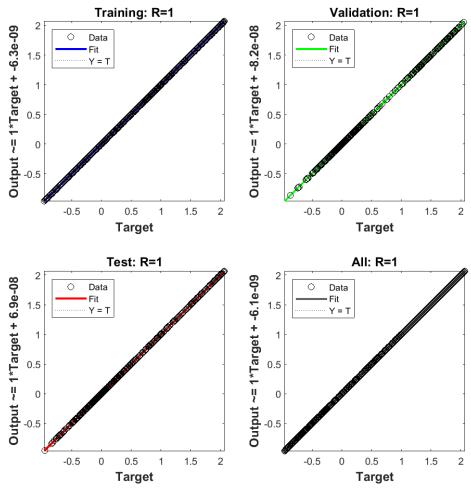

d) Regression plot about case 4

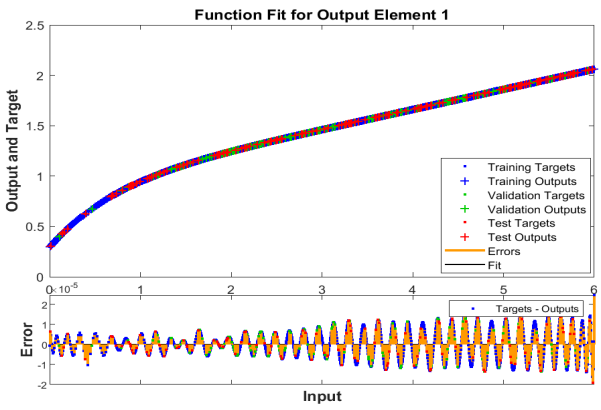

e) Function fit plot about case 4

Figure 9. Graphical outcomes of LMBNNA for case 4 of scenario 6 for 2D-SPCNFF.

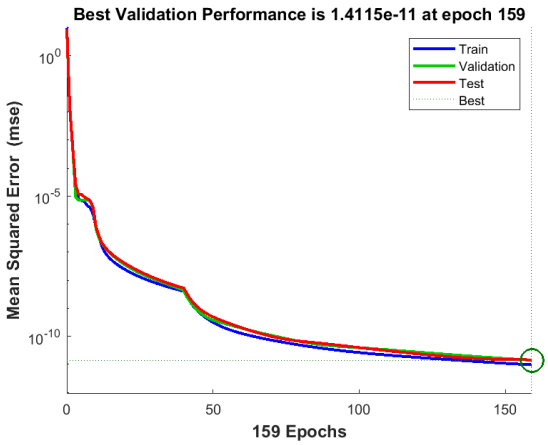

a) MSE of performance about case 2

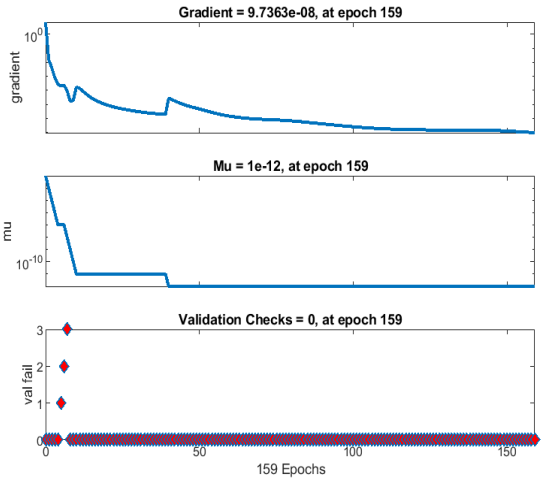

b) Gradient plot about case 2

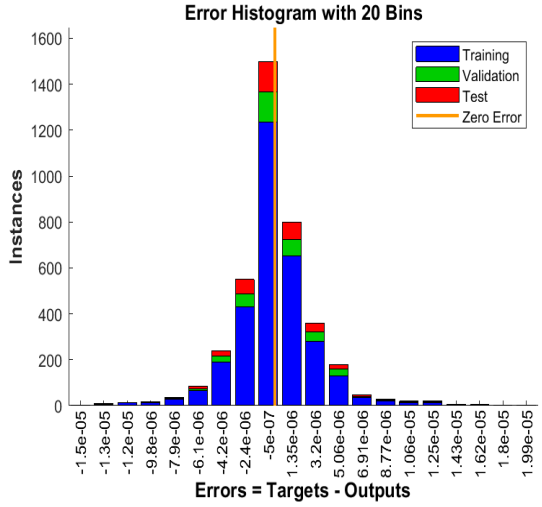

c) Error histogram plot about case 2

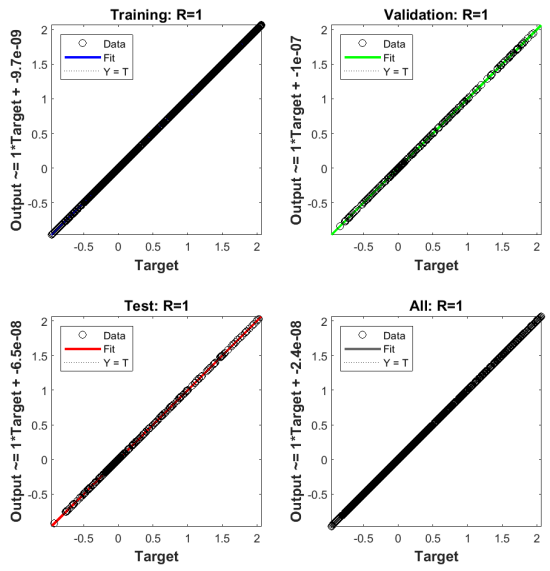

d) Regression plot about case 2

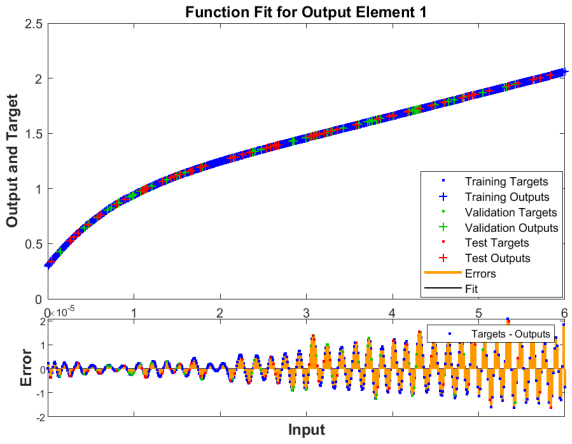

e) Function fit plot about case 2

Figure 10. Graphical outcomes of LMBNNA for case 2 of scenario 7 for 2D-SPCNFF.

Figures 11-13 present the conduct of the flux velocity $f'(\eta)$ fluid temperature $\theta(\eta)$, and fluid concentration $\phi(\eta)$ with the effects of various values of physical factors such the mixed convection parameter (λ), Hartmann number (M), Ecker number (Ec), activation energy parameter (E), radiation parameter (R), heat generating parameter (δ), and reaction rate ($\in$).

The flux velocity is reducing for bigger value of the Hartmann number while it is growing for rising value of the mixed convection

parameter as displayed in Figure **11(a-b).**

The temperature distribution is increasing regarding increasing value about the Ecker number, radiation parameter, and heat generating parameter as plotted in **Figure 12(a-c)**.

The fluid concentration is increasing for large value of activation energy parameter while it is decreasing for growing value of reaction rate that are shown in **Figure 13(a-b)**.

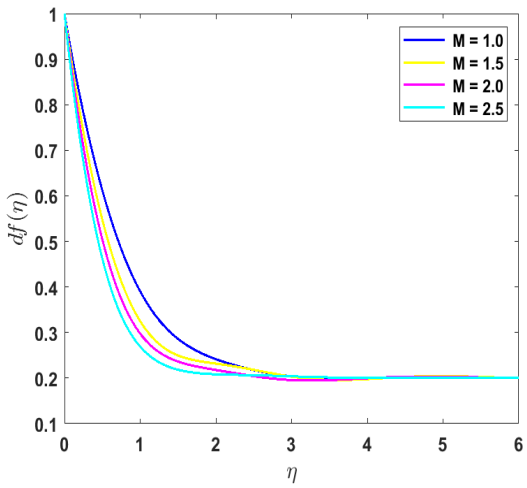

(a). Behavior of f' under impact M

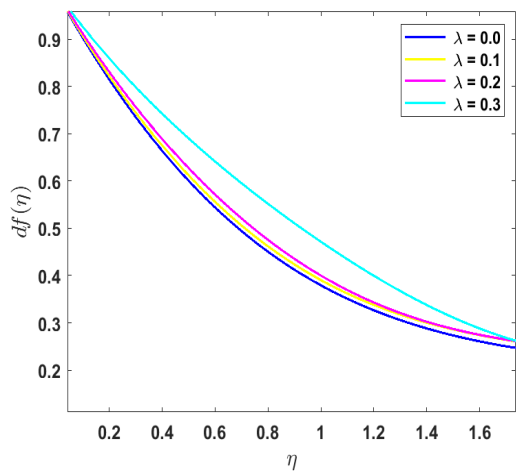

(b). Behavior of f' under impact λ

Figure 11. Behavior of flow velocity under impact Hartmann number and mixed convection parameter

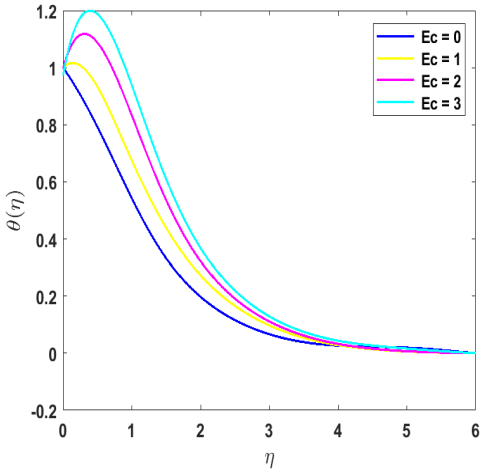

(a). Behavior of θ under impact E_c

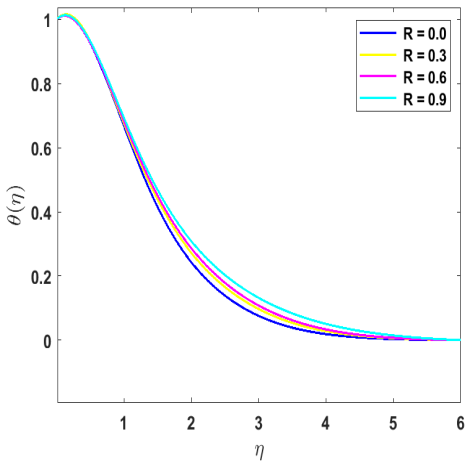

(b). Behavior of θ under impact R

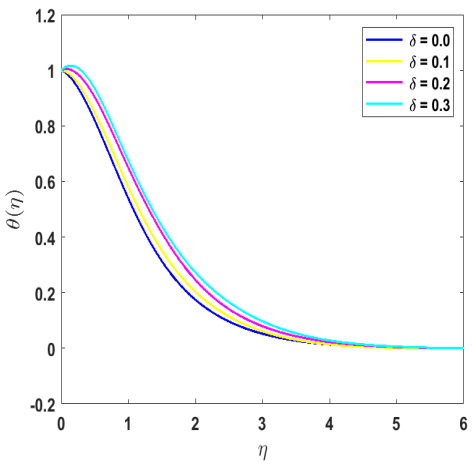

(c). Behavior of θ under impact δ

Figure 12. Behavior of the temperature distribution under impact the Ecker number, radiation parameter, and heat generating parameter

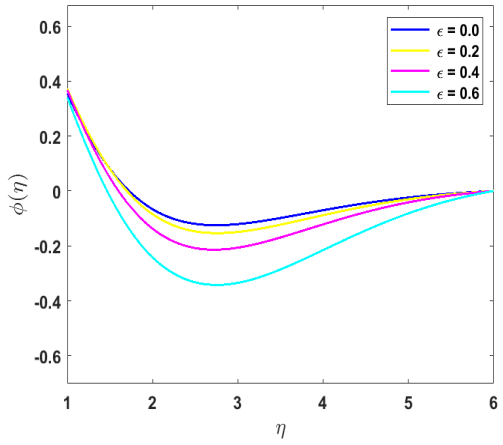

(a). Behavior of ϕ under impact $\in$

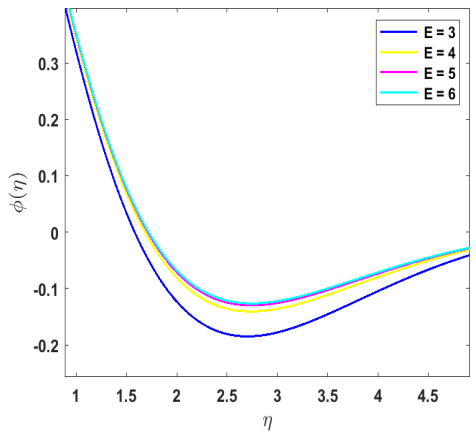

(b). Behavior of ϕ under impact E

Figure 13. Behavior of the concentration under impact the reaction rate and activation energy

CONCLUSION

The mathematical formulation of the two-dimensional stagnation point Carreau nanofluid flux 2D-SPCNFF subject to thermal radiation and activation energy is reviewed in this study by employing an innovative stochastic numerical technique dependent on a Levenberg Marquardt backpropagation neural networks approach LMBNNA. For the 2D-SPCNFF formulation, the nonlinear ordinary differential equations (ODEs) are found by simplifying the nonlinear partial differential equations (PDEs). The Lobatto IIIA technique would first solve ODEs for several physical factors to generate reference data. The convergence, stability, and accuracy of LMBNNA for 2D-SPCNFF are investigated using the mean squared error of performance, gradient results, mu values, histogram for error findings, and linear regression assessment. Under the influence of a wide range of different values about several physical parameters, the conduct of the flux velocity, fluid temperature, and fluid concentration is demonstrated.

The following is an overview about the study outcomes.

- In mean square error plots, the desired performance for the training, testing, and validation processes illustrates the stability of the suggested LMBNN approach.
- The gradient and mu parameter values, which can be observed in training state plots, provide an illustration of the recommended LMBNN approach converges.
- The error histogram and function fit plots show the error analysis of the LMBNN approach.
- If the Hartmann number increases, the flux velocity decreases but it rises when the mixed convection parameter increases.
- With rising heat generation parameter, radiation parameter, and Ecker number values, the temperature distribution grows.
- For large rate of an activation energy parameter, the concentration increases, whereas regarding large values of the reaction rate, it decreases.

In future work, use the suggested LMBNN approach for a number of problems involving nanofluids influenced by an **activation energy** (Shahid et al. (2022); Azam et al. (2022); Shahid et al. (2022); Habib et al. (2022)).

REFERENCES

[1] Mustafa, M., Khan, J. A., Hayat, T., and Alsaedi, A. (2017), "Buoyancy effects on the MHD nanofluid flow past a vertical surface with chemical reaction and activation energy", *International Journal of Heat and Mass Transfer*, Vol. 108, pp. 1340-1346.

[2] Hayat, T., Riaz, R., Aziz, A., and Alsaedi, A. (2020), "Influence of Arrhenius activation energy in MHD flow of third grade nanofluid over a nonlinear stretching surface with convective heat and mass conditions", *Physica A: Statistical Mechanics and its Applications*, Vol. 549, pp. 124006.

[3] Sajid, T., Sagheer, M., Hussain, S., and Bilal, M. (2018), "Darcy-Forchheimer flow of Maxwell nanofluid flow with nonlinear thermal radiation and activation energy", *AIP Advances*, Vol. 8 No. 3, pp. 035102.

[4] Khan, M. I., Khan, M. W. A., Alsaedi, A., Hayat, T., and Khan, M. I. (2020), "Entropy generation optimization in flow of non-Newtonian nanomaterial with binary chemical reaction and Arrhenius activation energy", *Physica A: Statistical Mechanics and its Applications*, Vol. 538, pp.122806.

[5] Alsaadi, F. E., Hayat, T., Khan, M. I., and Alsaadi, F. E. (2020), "Heat transport and entropy optimization in flow of magneto-Williamson nanomaterial with Arrhenius activation energy", *Computer Methods and Programs in Biomedicine*, Vol. 183, pp. 105051.

[6] Bhatti, M. M., Shahid, A., Abbas, T., Alamri, S. Z., and Ellahi, R. (2020), "Study of activation energy on the movement of gyrotactic microorganism in a magnetized nanofluids past a porous plate", *Processes*, Vol. 8 No. 3, pp. 328.

[7] Kalaivanan, R., Ganesh, N. V., and Al-Mdallal, Q. M. (2020), "An investigation on Arrhenius activation energy of second grade nanofluid flow with active and passive control of nanomaterials", *Case Studies in Thermal Engineering*, Vol. 22, pp. 100774.

[8] Howell, J. R., Mengüç, M. P., Daun, K., & Siegel, R. (2020), "Thermal radiation heat transfer", *CRC press*.

[9] Hussain, S., Raizah, Z., and Aly, A. M. (2022), "Thermal radiation impact on bioconvection flow of nano-enhanced phase change materials and oxytactic microorganisms inside a vertical wavy porous cavity", *International Communications in Heat and Mass Transfer*, Vol. 139, pp. 106454.

[10] Bilal, M., Saeed, A., Gul, T., Kumam, W., Mukhtar, S., and Kumam, P. (2022), "Parametric simulation of micropolar fluid with thermal radiation across a porous stretching surface", *Scientific Reports*, Vol. 12 No. 1, pp. 1-11.

[11] Waqas, H., Fida, M., Liu, D., Manzoor, U., and Muhammad, T. (2022), "Numerical simulation of entropy generation for nanofluid with the consequences of thermal radiation and Cattaneo-Christov heat flux model", *International Communications in Heat and Mass Transfer*, Vol. 137, pp. 106293.

[12] Shaw, S., Samantaray, S. S., Misra, A., Nayak, M. K., and Makinde, O. D. (2022), "Hydromagnetic flow and thermal interpretations of Cross hybrid nanofluid influenced by linear, nonlinear, and quadratic thermal radiations for any Prandtl number", *International Communications in Heat and Mass Transfer*, Vol. 130, pp. 105816.

[13] Ramzan, M., Shahmir, N., Alotaibi, H., Ghazwani, H. A. S., and Muhammad, T. (2022), "Thermal performance comparative analysis of nanofluid flows at an oblique stagnation point considering Xue model: A solar application", *Journal of Computational Design and Engineering*, Vol. 9 No. 1, pp. 201-215.

[14] Haq, R. U., Sajjad, T., Usman, M., and Naseem, A. (2022), "Oblique stagnation point flow of micropolar nanofluid impinge along a vertical surface via modified Chebyshev collocation method", *Physics of Fluids*, Vol. 34 No. 10, pp. 102001.

[15] Awan, A. U., Aziz, M., Ullah, N., Nadeem, S., and Abro, K. A. (2022), "Thermal analysis of oblique stagnation point flow with slippage on second-order fluid", *Journal of Thermal Analysis and Calorimetry*, Vol. 147 No. 5, pp. 3839-3851.

[16] Bai, Y., Wang, X., and Zhang, Y. (2022), "Unsteady oblique stagnation-point flow and heat transfer of fractional Maxwell fluid with convective derivative under modified pressure field", *Computers & Mathematics with Applications*, Vol. 123, pp. 13-25.

[17] Hussain, S. M., Goud, B. S., Madheshwaran, P., Jamshed, W., Pasha, A. A., Safdar, R., ... and Ahmad, M. K. (2022), "Effectiveness of nonuniform heat generation (sink) and thermal characterization of a carreau fluid flowing across a nonlinear elongating cylinder: A numerical study", *ACS omega*, Vol. 7 No. 29, pp. 25309-25320.

[18] Rehman, K. U., Shatanawi, W., and Abodayeh, K. (2022), "A group theoretic analysis on heat transfer in MHD thermally slip Carreau fluid subject to multiple flow regimes (MFRs)", *Case Studies in Thermal Engineering*, Vol. 30, pp. 101787.

[19] Reedy, S., Srihari, P., Ali, F., and Naikoti, K. (2022), "Numerical analysis of Carreau fluid flow over a vertical porous microchannel with entropy generation", *Partial Differential Equations in Applied Mathematics*, Vol. 5, pp. 100304.

[20] Qayyum, M., Abbas, T., Afzal, S., Saeed, S. T., Akgül, A., Inc, M., ... and Alsubaie, A. S. (2022), "Heat Transfer Analysis of Unsteady MHD Carreau Fluid Flow over a Stretching/Shrinking Sheet", *Coatings*, Vol. 12 No. 11, pp. 1661.

[21] Shoaib, M., Naz, S., Raja, M. A. Z., Aslam, S., Ahmad, I., and Nisar, K. S. (2022), "A design of soft computing intelligent networks for MHD Carreau nanofluid model with thermal radiation", *International Journal of Modern Physics B*, Vol. 36 No. 27, pp. 2250192.

[22] Uddin, I., Ullah, I., Raja, M. A. Z., Shoaib, M., Kiani, A. K., and Islam, S. (2022), "Thin film flow of carreau nanofluid over a stretching surface with magnetic field: Numerical treatment with intelligent computing paradigm", *International Journal of Modern Physics B*, Vol. 36 No. 03, pp. 2250021.

[23] Choi, S. U., & Eastman, J. A. (1995), "Enhancing thermal conductivity of fluids with nanoparticles (No. ANL/MSD/CP-84938; CONF-951135-29), *Argonne National Lab. (ANL), Argonne, IL (United States).*

[24] Zaman, A., & Khan, A. A. (2021), "Time dependent non-Newtonian nano-fluid (blood) flow in w-shape stenosed channel; with curvature effects", *Mathematics and Computers in Simulation*, Vol. 181, pp. 82-97.

[25] Uddin, S., Mohamad, M., Rahimi-Gorji, M., Roslan, R., and Alarifi, I. M. (2020), "Fractional electro-magneto transport of blood modeled with magnetic particles in cylindrical tube without singular kernel", *Microsystem Technologies*, Vol. 26 No. 2, pp. 405-414.

[26] Shoaib, M., Abukhaled, M., Raja, M. A. Z., Khan, M. A. R., Sabir, M. T., Nisar, K. S., and Iltaf, I. (2022), "Heat and mass transfer analysis for unsteady three-dimensional flow of hybrid nanofluid over a stretching surface using supervised neural networks", *Frontiers in Physics*, Vol. 10, pp. 949907.

[27] Hamid, A., Chu, Y. M., Khan, M. I., Kumar, R. N., Gowd, R. P., and Prasannakumara, B. C. (2021), "Critical values in axisymmetric flow of magneto-Cross nanomaterial towards a radially shrinking disk", *International Journal of Modern Physics B*, Vol. 35 No. 07, pp. 2150105.

[28] Shoaib, M., Naz, S., Nisar, K. S., Raja, M. A. Z., Aslam, S., and Ahmad, I. (2022), "MHD Casson Nanofluid in Darcy-Forchheimer Porous Medium in the Presence of Heat Source and Arrhenious Activation Energy: Applications of Neural Networks", *International Journal of Modelling and Simulation*, pp. 1-24.

[29] Ilyas, H., Ahmad, I., Raja, M. A. Z., Tahir, M. B., and Shoaib, M. (2021), "Intelligent computing for the dynamics of fluidic system of electrically conducting Ag/Cu nanoparticles with mixed convection for hydrogen possessions", *International Journal of Hydrogen Energy*, Vol. 46 No. 7, pp. 4947-4980.

[30] Ilyas, H., Ahmad, I., Raja, M. A. Z., Tahir, M. B., and Shoaib, M. (2021), "Intelligent networks for crosswise stream nanofluidic model with Cu–H2O over porous stretching medium", *International Journal of Hydrogen Energy*, Vol. 46 No. 29, pp. 15322-15336.

[31] Uddin, I., Ullah, I., Raja, M. A. Z., Shoaib, M., Islam, S., and Muhammad, T. (2021), "Design of intelligent computing networks for numerical treatment of thin film flow of Maxwell nanofluid over a stretched and rotating surface", *Surfaces and Interfaces*, Vol. 24, pp. 101107.

[32] Ijaz Khan, M., Qayyum, S., Nigar, M., Chu, Y. M., and Kadry, S. (2020), "Dynamics of Arrhenius activation energy in flow of Carreau fluid subject to Brownian motion diffusion", *Numerical Methods for Partial Differential Equations*.

[33] Hayat, T., Qayyum, S., Waqas, M., and Ahmed, B. (2017), "Influence of thermal radiation and chemical reaction in mixed convection stagnation point flow of Carreau fluid", *Results in physics*, Vol. 7, pp. 4058-4064.

[34] Shahid, A., Bhatti, M. M., Ellahi, R., and Mekheimer, K. S. (2022), "Numerical experiment to examine activation energy and bi-convection Carreau nanofluid flow on an upper paraboloid porous surface: Application in solar energy", *Sustainable Energy Technologies and Assessments*, Vol. 52, pp. 102029.

[35] Azam, M., Mabood, F., and Khan, M. (2022), "Bioconvection and activation energy dynamisms on radiative sutterby melting nanomaterial with gyrotactic microorganism", *Case Studies in Thermal Engineering*, Vol. 30, pp. 101749.

[36] Shahid, A., Bhatti, M. M., Ellahi, R., and Mekheimer, K. S. (2022), "Numerical experiment to examine activation energy and bi-convection Carreau nanofluid flow on an upper paraboloid porous surface: Application in solar energy", *Sustainable Energy Technologies and Assessments*, Vol. 52, pp. 102029.

[37] Habib, D., Salamat, N., Abdal, S., Siddique, I., Ang, M. C., and Ahmadian, A. (2022), "On the role of bioconvection and activation energy for time dependent nanofluid slip transpiration due to extending domain in the presence of electric and magnetic fields", *Ain Shams Engineering Journal*, Vol. 13 No. 1, pp. 101519.